PHYSICAL REVIEW B **69**, 241403(R) (2004)

Single- and double-resonance Raman *G*-band processes in carbon nanotubes

M. Souza,[1] A. Jorio,[1] C. Fantini,[1] B. R. A. Neves,[1] M. A. Pimenta,[1] R. Saito,[2] A. Ismach,[3] E. Joselevich,[3] V. W. Brar,[4] Ge. G. Samsonidze,[5] G. Dresselhaus,[6] and M. S. Dresselhaus[4,5]

[1]*Departamento de Física, Universidade Federal de Minas Gerais, Belo Horizonte, MG, 30123-970 Brazil*

[2]*Department of Physics, Tohoku University and CREST JST, Sendai 980-8578, Japan*

[3]*Department of Materials and Interfaces, Weizmann Institute of Science, Rehovot 76100, Israel*

[4]*Department of Physics, Massachusetts Institute of Technology, Cambridge, Massachusetts 02139-4307, USA*

[5]*Department of Electrical Engineering and Computer Science, Massachusetts Institute of Technology, Cambridge, Massachusetts 02139-4307, USA*

[6]*Francis Bitter Magnet Laboratory, Massachusetts Institute of Technology, Cambridge, Massachusetts 02139-4307, USA*

(Received 2 February 2004; revised manuscript received 3 May 2004; published 23 June 2004)

This work reports Raman spectroscopy measurements from single wall carbon nanotubes (SWNTs) addressing the nature of the *G*-band resonance Raman spectra. Experimental results on different samples are presented, i.e., aligned and misaligned SWNT samples, as well as isolated and bundled SWNTs. It is shown that the Raman spectra from nondefective SWNTs, both isolated and bundled, are composed of strong first-order single resonance Raman features. Defective materials, however, are found to exhibit lower intensity spectra with contributions from both single resonance and defect-induced double resonance features.

DOI: 10.1103/PhysRevB.69.241403 PACS number(s): 78.30.Na, 78.20.Bh, 78.66.Tr, 63.22.+m

Raman spectroscopy is one of the most powerful techniques for studying carbon nanotubes.[1–3] The so-called *G*-band, appearing in the frequency range from 1520 to 1630 cm^{-1} (roughly centered at the 1582 cm^{-1} graphite frequency), contains multiple components and gives a clear spectroscopic signature of carbon nanotubes. The frequencies of the various *G*-band peaks exhibit a clear and well-established dependence on diameter (d_t), as well as a dependence on whether the nanotube is metallic or semiconducting.[1–4] Even though the *G*-band Raman modes have been widely used for many years for the study and characterization of carbon nanotube samples, the nature of the scattering process for the *G*-band in nanotubes is still under debate.

The debate concerns whether the Raman signal from the *G*-band in SWNTs originates from a single-resonance first-order Raman process (light absorption, $q \approx 0$ phonon emission/absorption, light emission)[1–3,5] or from a defect-induced double resonance Raman process (light absorption, $q \neq 0$ phonon emission/absorption, scattering by a defect, light emission).[6–8] This simple and fundamental issue is of major importance for the physics of carbon nanotubes. There are several SWNT Raman features that are well established as defect-induced double resonance features, e.g., the *D* band,[1–3] the acoustic modes and the *D** band ($\sim$1620 cm^{-1}),[9] and these features can only be observed in the presence of defects. The question then arises whether, by assigning the origin of the Raman signal from the *G*-band in SWNTs to a defect-induced double resonance effect, would one then never observe a strong *G*-band Raman spectrum from a nondefective carbon nanotube? Would the radial breathing mode (RBM) feature, largely used for SWNT diameter characterization,[1–3] then also be connected to defect-induced double resonance processes?[10] Answering these questions is important, since their answers have a strong influence on how Raman spectroscopy can be used to characterize SWNTs. Answering these questions is the goal of this paper that provides a consistent picture to explain present and previous experimental results concerning this debate.

Micro-Raman spectra were recorded in a backscattering configuration using both single and triple monochromators, equipped with cooled charge coupled devices (CCDs), by using different excitation laser lines. The spectra were recorded from different samples: (i) a fiber of an aligned SWNT bundle,[11] with an overall diameter of $\sim$1 mm size and the nanotubes in the sample ($d_t = 1.3 \pm 0.2$ nm) exhibiting exceptionally good alignment along the fiber axis (better than $\pm 5°$);[12] (ii) isolated nanotubes on a Si/SiO_2 substrate with a random orientation,[13] low tube density, and a diameter range $1 < d_t < 2$ nm; (iii) isolated nanotubes on a sapphire substrate prepared so that the SWNTs are all aligned, and with a diameter range $0.7 < d_t < 1.7$ nm.[14] The Raman spectra are fit using a sum of Lorentzian peaks. For isolated SWNT measurements, atomic force microscopy (AFM) imaging of some samples was carried out to locate isolated SWNTs that could be further measured with resonance Raman spectroscopy. The AFM measurements were made with a Nanoscope IV MultiMode SPM from Veeco Instruments operating in the intermittent contact (Tapping) mode, using standard Si probes.

Figure 1 shows the *G*-band Raman spectra obtained from a SWNT fiber at two different locations, as shown in the inset to the upper panel. The upper spectrum comes from location **1**, at the center of the fiber, and it has been acquired with both incident and scattered light polarized along the fiber axis, i.e., the (ZZ) configuration. At this location, the cross-polarized (XX) spectra are $\sim$120 times less intense than the (ZZ) spectra, due to the antenna effect,[1–3] indicating an excellent degree of alignment for the SWNT bundles. The (ZZ) spectra can be fit using two sharp Lorentzians (11 cm^{-1} FWHM) located at $\omega_{G^-} = 1564$ cm^{-1} and $\omega_{G^+} = 1593$ cm^{-1}, while the (XX) spectra, although less intense, clearly exhibit

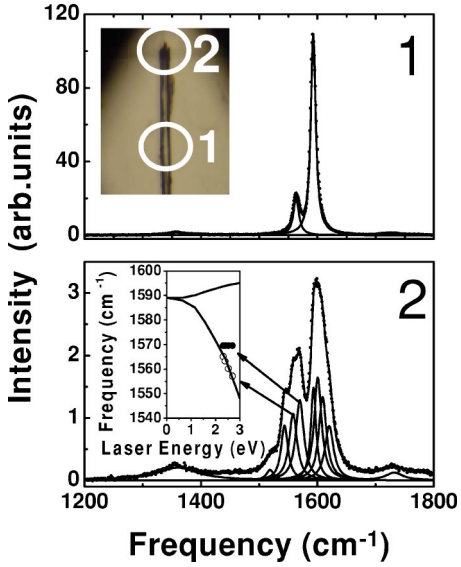

FIG. 1. (Color online) *G*-band resonance Raman spectrum from a fiber of aligned SWNT bundles (E_{laser}=2.71 eV). The inset to the upper panel shows an optical image of the sample. The spectrum in the upper panel was taken from location **1** (see upper inset) with the (ZZ) polarization scattering geometry, and the spectrum in the lower panel was acquired from location **2**. The inset to the lower panel shows the E_{laser} dependence of the two peaks indicated by arrows. The solid curves in this inset are predictions for the E_{laser} dependence of the *G*-band double resonance features (Refs. 6 and 7).

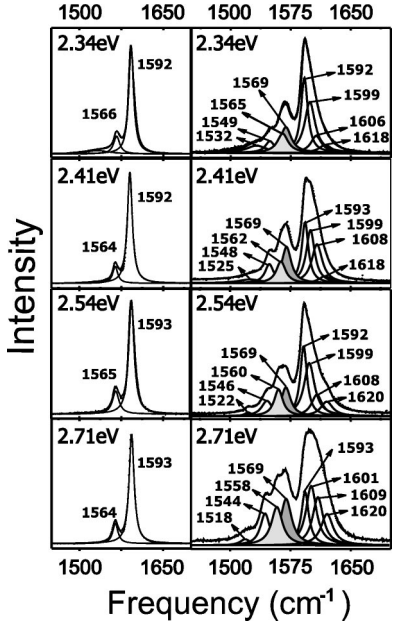

FIG. 2. The left panels show the *G*-band Raman spectra in the (ZZ) polarization geometry at location **1** [see inset in Fig. 1(a)], using four different laser energies, as displayed in the figure. The right panels show the spectra measured with the same laser energies in location **2** of the sample. The peak frequencies are displayed in cm^{-1}.

contributions from the E_2 symmetry features, as previously discussed.[1–3,15] The well-known disorder-induced *D*-band is almost absent, the integrated *D*-band area being ~35 times smaller than the integrated area of the *G*-band Lorentzian peaks.

The lower panel of Fig. 1 shows the *G*-band spectrum from location **2**, which is at the edge of the same fiber, where misalignment and defects (structural and impurities) are expected. The *G*-band intensity is much lower in location **2**, about 35 times less intense than in location **1**. Many peaks are observed in the spectrum at location **2**, clearly different from the spectrum at location **1**. Eight Lorentzian peaks are used for fitting the spectra at location **2**. Four lower frequency G^- peaks can be clearly distinguished in the spectrum. Four upper frequencies G^+ peaks were used, since it is expected that the same number of G^+ and G^- peaks will be related independently to the LO and to the TO branches of 2D graphite, respectively, on the basis of the model (either single or double resonance) used to explain the multipeak feature.[1–3,7] The integrated area for the *D*-band in location **2** is only 3 times smaller than in location **1**, the *D*-band in location **2** being relatively much more intense than in location **1** when compared with the *G* band intensity. The Lorentzian peaks used to fit the *D* and *G* bands in location **2** exhibit similar integrated areas.

Figure 2 shows similar spectra to those shown in Fig. 1, but taken with different E_{laser} lines. The left panels come from location **1** and exhibit no significant dependence on E_{laser}. The right panels come from location **2**, and interestingly, some of the peaks are dispersive, while some are not. For example, the dark gray peak does not change frequency when E_{laser} is changed, while the light gray peak down-shifts with increasing E_{laser}. The E_{laser} dependence for these two gray colored peaks is shown in the lower inset to Fig. 1 (points) together with predictions from the double resonance model (lines).[6,7]

Based on the experimental results in Figs. 1 and 2, the assignment of the scattering nature for the *G*-band peaks can be discussed. The (ZZ) spectrum obtained in location **1**, the region of aligned defect-free SWNTs in the SWNT fiber (see Fig. 1), exhibits two sharp peaks. This result is in agreement with group theory predictions for first-order Raman scattering using this scattering configuration, where only two *A* symmetry modes are expected to be Raman active.[1–3,15] Considering the average tube diameter of d_t=1.3 nm, the *G*-band Lorentzian frequencies (1565 and 1593 cm^{-1}) are also in agreement with the expected results for the *A* modes in carbon nanotubes.[1–3,5] Furthermore, these features are not E_{laser} dispersive (see left panels of Fig. 2). Therefore, they are assigned as first-order single resonance Raman features.

The spectra obtained in location **2**, where defects and misalignment are expected, clearly show results that cannot be explained by only considering first-order Raman-allowed modes, even considering that the *G*-band is composed of 6 peaks and contribution from different SWNTs within the bundles. Eight peaks are observed, some of the peaks are dispersive, while some of the peaks are not dispersive, as shown in the lower inset to Fig. 1 and in Fig. 2. These spectra can be explained as composed of both first-order single resonance Raman peaks *and* defect-induced double resonance features.

Considering electronic transitions occurring at E_{laser}

=2.41 eV, the difference between the single and double resonance frequencies are estimated to be about 8 cm^{-1} for E_1 symmetry phonons, and 4 cm^{-1} for E_2 symmetry phonons.[1,6] Therefore, the G^- peaks observed in the spectra from location **2**, and shown in Figs. 1 and 2, are assigned as follows: the peak at 1569 cm^{-1} is assigned to a E_1 single resonance process; the peak at ~1562 cm^{-1} to a double resonance process; these peaks are separated by 7 cm^{-1} for E_{laser} =2.41 eV, in agreement with the estimated 8 cm^{-1}. The peak at ~1546 cm^{-1} is assigned to unresolved double and single resonance E_2 symmetry modes. Finally, using the zone folding picture, the ~20 cm^{-1} splitting between the 1548 cm^{-1} and the 1525 cm^{-1} features agrees with the frequency splitting expected for the E_2 and E_3 symmetry modes. In this case, the 1525 cm^{-1} feature can be assigned to an E_3 symmetry disorder-induced peak.[16]

With increasing laser energy, the splitting between the single and double resonance features is expected to increase.[6] This behavior is clearly observed for the two G^- features shown in Fig. 2 by gray colored Lorentzians. The upper frequency first-order single resonance feature always appears at 1569 cm^{-1}, in agreement with previous experimental[5] and theoretical[17] results for the E_1 symmetry mode. The light gray peak (assigned as a double resonance feature) downshifts from 1565 to 1558 cm^{-1} when E_{laser} is increased from 2.34 eV up to 2.71 eV. The frequency behavior of the light gray peak exhibits the dispersive behavior expected for a double resonance feature, considering the results to be an average over contributions from many different nanotubes within the bundle.[6,7]

A small dispersive behavior has also been observed for the E_2 and E_3 peaks. These small dispersive behaviors could be consistently fit by using one nondispersive peak, and one dispersive peak obeying the double resonance prediction. However, as discussed above, the two features are too close in frequency and they cannot be clearly distinguished in the experimental spectra.

A fitting analysis for the high frequency upper G^+ feature is hard to make, since the peaks all overlap with each other. This overlap of several features can be understood for both single and double resonance features based on a zone folding picture, since close to the Γ point the dispersion of the LO phonon branch in 2D graphite is small when compared with the dispersion of the TO phonon branch. The G^+ feature was fit using four Lorentzians for consistency with G^-. These data show a tendency to upshift as E_{laser} is increased, consistent with a contribution to the G^+ feature from double resonance features. However, the dispersion of these data cannot be described by that predicted by the double resonance model, because the G^+ feature has unresolved contributions from both single and double resonance processes.

From the arguments developed here, the analysis of the E_{laser} dependence of the *G*-band feature from defective materials requires both single and double resonance contributions to achieve a consistent fit. This result explains why previously published work did not show the correct dispersion for the double resonance feature.[7] By considering the *G*-band spectra from defective SWNTs to originate only from double resonance processes, no detailed analysis could be carried out.

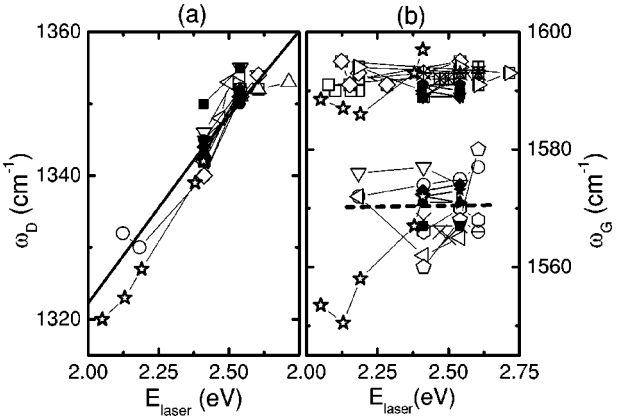

FIG. 3. The *D* (a), G^- and G^+ (b) band frequencies observed for different isolated nanotubes on a sapphire substrate (open symbols) and on a Si/SiO_2 substrate (filled symbols) using several different laser lines. The stars symbol data points come from Ref. 8. The dark solid line in (a) shows the prediction from the double resonance model for the *D*-band ω_D. The solid line was downshifted to fit the experimental results according to Ref. 18.

It is important also to discuss results on isolated SWNT samples. Figure 3 shows data for ω_D (a), ω_{G^+} and ω_{G^-} (b) as a function of E_{laser} for 11 different spot positions, i.e., 11 different isolated SWNTs, six isolated SWNTs on top of a sapphire substrate (open symbols), and 5 SWNTs on top of a Si/SiO_2 substrate (filled symbols), plus one set of data (stars) from Ref. 8. Each set of points connected by lines comes from one individual different SWNT.

The solid line in Fig. 3(a) represents the prediction from the double resonance model for the *D* band.[6,7] In general, the experimentally observed ω_D follows the prediction from the double resonance model very well. The *G*-band spectra from the same SWNT are sometimes observed to change slightly from one E_{laser} to the other. Effects of local temperature and selection rules related to tuning through different resonance conditions should be considered. For example, when $E_\mu \rightarrow E_\mu$ or $E_\mu \rightarrow E_{\mu\pm1}$ electronic transitions are excited, different phonons are selected.[5] Such an effect can give rise to different first-order single resonance Raman spectra when making measurements with different E_{laser} lines, since for each E_{laser}, phonons with different symmetries could be activated. These small changes could also be due to contributions from both single and double resonance features, as discussed for defective SWNT bundles, while the various individual SWNTs exhibit different defects or no defect, different resonance and extrinsic environmental states. The dashed line in Fig. 3(b) however shows a linear fit considering all the G^- peaks (excluding the stars for a metallic SWNT from Ref. 8), and a straight line gives the best average behavior. Once the G^- frequency is predicted by double resonance to decrease with increasing E_{laser} (exception for the special case of the metallic SWNT discussed in Ref. 8), the resonance signal from isolated SWNTs measured here shows no clear evidence for a defect-induced double resonance mechanism.

In conclusion, a consistent picture that explains present and previously reported results for the scattering nature of

the *G*-band of SWNTs is presented. Basically, the *G*-band in defect-free aligned SWNTs originates from single resonance processes, thus implying that the knowledge developed from the first-order single resonance *G*-band Raman spectra can be used for the characterization of high quality samples. The *G*-band in defective SWNT samples, however, can exhibit different peaks, originating from both single and double resonance processes, and they have been assigned here for SWNT bundles. Both single resonance and double resonance features are found to exhibit contributions of similar intensity to the spectra of defective materials, the extra resonance in the double resonance process allowing observation of an effect one order higher in perturbation theory. Therefore, a complete analysis involving both single and double resonance features must be developed to understand their *G*-band spectra. Interestingly, it turns out that the averaged results from SWNT bundles deliver illuminating messages leading to a clearer answer for the importance of the single and double resonance nature of the *G*-band scattering processes in SWNTs, while in the case of isolated SWNTs, much care must be taken in the analysis, since different single resonance conditions select different symmetry modes and different defects could lead to a different double resonance spectrum.

Finally, it is important to comment that for the RBM feature, no significant E_{laser} dependence or differences between RBM spectra from locations **1** and **2** at the SWNT fiber have been observed. Up to now there is no evidence for a double resonance behavior for the RBM feature in the literature, neither from bundles nor from isolated SWNTs. The questions raised at the beginning of this text can be answered: A perfect carbon nanotube should exhibit strong first-order single resonance *G*-band and RBM features.

The authors acknowledge Professors J. H. Hafner and C. M. Lieber for the SWNTs on Si/SiO_2 samples, and Professor K. I. Winey and R. Haggenmueller for SWNT/poly(methylmethacrylate) composite fibers. The authors also acknowledge Professor A. G. Rinzler for kindly providing his SWNT samples. Work supported by the CNPq/NSF program (NSF INT 00-00408 and CNPq 910120/99-4) and Instituto de Nanociências, Brazil. A.J. has financial support from PRPq-UFMG. The MIT authors acknowledge support under NSF DMR 01-16042. R.S. acknowledges a Grant-in-Aid (No. 13440091) from the Ministry of Education, Japan. E.J., A.I., and G.D. acknowledge support from the U.S.-Israel Binational Science Foundation (Grant No. 2000218).

[1] M. S. Dresselhaus and P. C. Eklund, Adv. Phys. **49**, 705 (2000), and references therein.

[2] M. S. Dresselhaus, G. Dresselhaus, A. Jorio, A. G. Souza Filho, and R. Saito, Carbon **40**, 2043 (2002), and references therein.

[3] A. Jorio, M. A. Pimenta, A. G. Souza Filho, R. Saito, G. Dresselhaus, and M. S. Dresselhaus, New J. Phys. **5**, 139 (2003), and references therein.

[4] M. A. Pimenta, A. Marucci, S. Empedocles, M. G. Bawendi, E. B. Harlon, A. M. Rao, P. C. Eklund, R. E. Smalley, G. Dresselhaus, and M. S. Dresselhaus, Phys. Rev. B **58**, R16016 (1998).

[5] A. Jorio, M. A. Pimenta, A. G. Souza Filho, Ge. G. Samsonidze, A. K. Swan, M. S. Ünlü, B. B. Goldberg, R. Saito, G. Dresselhaus, and M. S. Dresselhaus, Phys. Rev. Lett. **90**, 107403 (2003).

[6] R. Saito, A. Jorio A. G. Souza Filho, G. Dresselhaus, M. S. Dresselhaus, and M. G. Pimenta, Phys. Rev. Lett. **88**, 027401 (2002).

[7] J. Maultzsch, S. Reich, and C. Thomsen, Phys. Rev. B **65**, 233402 (2002).

[8] J. Maultzsch, S. Reich, U. Schlecht, and C. Thomsen, Phys. Rev. Lett. **91**, 087402 (2003).

[9] P.-H. Tan, L. An, L.-Q. Liu, Z.-X. Guo, R. Czerw, D. L. Carroll, P. M. Ajayan, N. Zhang, and H. L. Guo, Phys. Rev. B **66**, 245410 (2002).

[10] C. Thomsen, J. Maultzsch, and S. Reich, in *Nanomolecular Nanostructure, IAP Conference Proceedings of the XVII International Winter school/Euroconference on Electronic Properties of Novel Materials*, Kirchberg, Tirol, Austria, 2003, edited by H. Kuzmany, J. Fink, M. Mehring, and S. Roth, Vol. 685, p. 225.

[11] R. Haggenmueller, H. H. Gommans, A. G. Rinzler, J. E. Fisher, and K. I. Winey, Chem. Phys. Lett. **330**, 219 (2000).

[12] J. Hwang, H. H. Gommans, A. Ugawa, H. Tashiro, R. Haggenmueller, K. I. Winey, J. E. Fischer, P. B. Tanner, and A. G. Rinzler, Phys. Rev. B **62**, R13310 (2000).

[13] J. Hafner, C. L. Cheung, T. H. Oosterkamp, and C. M. Lieber, J. Phys. Chem. B **105**, 743 (2001).

[14] A. Ismach and E. Joselevich (unpublished).

[15] A. Jorio, G. Dresselhaus, M. S. Dresselhaus, M. Souza, M. S. S. Dantas, M. A. Pimenta, A. M. Rao, R. Saito, C. Liu, and H. M. Cheng, Phys. Rev. Lett. **85**, 2617 (2000).

[16] It is important to stress that the symmetry identifications become less clear for higher order defect-induced scattering processes. However, the use of cutting lines and cutting line indices [see, Ge. G. Samsonidze, R. Saito, A. Jorio, M. A. Pimenta, A. G. Souza Filho, F. A. Grüneis, G. Dresselhaus, and M. S. Dresselhaus, J. Nanosci. Nanotechnol. **3**, 431 (2003)] simplifies the symmetry identification in the different scattering processes.

[17] O. Dubay, G. Kresse, and H. Kuzmany, Phys. Rev. Lett. **88**, 235506 (2002).

[18] A. G. Souza Filho, A. Jorio, Ge. G. Samsonidze, G. Dresselhaus, M. A. Pimenta, M. S. Dresselhaus, A. K. Swan, M. S. Ünlü, B. B. Goldberg, and R. Saito, Phys. Rev. B **67**, 035427(1–7) (2003).